

Metabolomic profiling identifies a novel mechanism for heat stroke-related acute kidney injury

LING XUE^{1*}, WENLI GUO^{2*}, LI LI², SANTA O U², TINGTING ZHU²,
LIANG CAI³, WENFEI DING² and WEIHUA WU²

Departments of ¹Urology and ²Nephrology, Sichuan Clinical Research Center for Nephropathy, The Affiliated Hospital of Southwest Medical University; ³Department of Nuclear Medicine, The Affiliated Hospital of Southwest Medical University, Luzhou, Sichuan 646000, P.R. China

Received April 13, 2020; Accepted August 20, 2020

DOI: 10.3892/mmr.2021.11880

Abstract. Heat stroke can induce a systemic inflammatory response, which may lead to multi-organ dysfunction including acute kidney injury (AKI) and electrolyte disturbances. To investigate the pathogenesis of heat stroke (HS)-related AKI, a mouse model of HS was induced by increasing the animal's core temperature to 41°C. Blood samples obtained from the tail vein were used to measure plasma glucose and creatinine levels. Micro-positron emission tomography-computed tomography (micro-PET/CT), H&E staining and transmission electron microscopy were conducted to examine metabolic and morphological changes in the mouse kidneys. Immunohistochemistry (IHC) and western blot analyses were performed to investigate the expression of apoptosis-inducing

factor mitochondria-associated 2 (Aifm2), high-mobility group box 1 (HMGB1) and receptor for advanced glycosylation end products (RAGE). Liquid chromatography-mass spectrometry analysis was conducted to find differential metabolites and signaling pathways. The HS mouse model was built successfully, with significantly increased creatinine levels detected in the serum of HS mice compared with controls, whereas micro-PET/CT revealed active metabolism in the whole body of HS mice. H&E and TUNEL staining revealed that the kidneys of HS mice exhibited signs of hemorrhage and apoptosis. IHC and western blotting demonstrated significant upregulation of Aifm2, HMGB1 and RAGE in response to HS. Finally, 136 differential metabolites were screened out, and enrichment of the 'biosynthesis of unsaturated fatty acids' pathway was detected. HS-associated AKI is the renal manifestation of systemic inflammatory response syndrome, and may be triggered by the HMGB1/RAGE pathway. Metabolomics indicated increased adrenic acid, docosahexaenoic acid and eicosapentaenoic acid may serve as metabolic biomarkers for AKI in HS. The findings suggested that a correlation between the HMGB1/RAGE pathway and biosynthesis of unsaturated fatty acids may contribute to the progression of HS-related AKI.

Correspondence to: Dr Weihua Wu, Department of Nephrology, Sichuan Clinical Research Center for Nephropathy, The Affiliated Hospital of Southwest Medical University, 25 Taiping Street, Luzhou, Sichuan 646000, P.R. China
E-mail: 12390369@qq.com

*Contributed equally

Abbreviations: ¹⁸FDG, ¹⁸F-deoxyglucose; ALS, amyotrophic lateral sclerosis; AKI, acute kidney injury; ARF, acute renal failure; DIC, disseminated intravascular coagulation; DHA, docosahexaenoic acid; EHS, exertional heat stroke; EPA, eicosapentaenoic acid; HMGB1, high-mobility group box 1; HS, heat stroke; IHC, immunohistochemistry; LC-MS, liquid chromatography-mass spectrometry; LPS, lipopolysaccharides; micro-PET/CT, micro-positron emission tomography-computed tomography; MODS, multiple organ dysfunction syndrome; NEHS, non-exertional HS; OPLS-DA, orthogonal partial least squares discriminant analysis; PCA, principal component analysis; RAGE, receptor for advanced glycosylation end products; SIRS, systemic inflammatory response syndrome; TEM, transmission electron microscopy

Key words: heat stroke, metabolomics, acute kidney injury, unsaturated fatty acids, HMGB1, RAGE

Introduction

Heat stroke (HS) is a potentially fatal medical condition, and its incidence and mortality rates are predicted to increase due to global warming (1). Between 2006 and 2010, ~3,000 HS-related deaths were reported in the USA according to an epidemiological analysis (2). In 2003, ~30,000 HS-related deaths were caused by a European heat wave event (3). Additionally, ~1,600 HS-related deaths are reported in India annually (4). A study estimated that HS-related deaths could increase to ~2.5 times the current rate (5).

HS is characterized by a core body temperature in excess of 40°C, skin that feels hot and dry to the touch, dysfunction of the central nervous system and occasionally multiple organ dysfunction syndrome (MODS) (6-8). HS is classified into exertional HS (EHS) and non-exertional HS (NEHS). EHS primarily affects young individuals who perform physical activities in high temperature and humid environments, such

as soldiers and athletes, whereas NEHS primarily affects elderly individuals, or those with preexisting conditions such as diabetes and heart disease (9). Regardless of the type, HS affects the temperature regulation system of the body, triggering damage to important body organs, such as the lungs, liver, brain and kidneys (10-12); this series of events may progress to MODS and induce death. The most common complication of HS is acute kidney injury (AKI), which can rapidly develop into acute renal failure (ARF), with a high mortality (13,14).

Although advances in medical science have resulted in the development of effective treatment/management strategies, such as rapid cooling, blood purification to stabilize organ functions and supportive therapies, the incidence and mortality rates of severe HS have not decreased in previous decades (15-17). A number of studies have identified certain biochemical markers as prognostic factors for HS. For example, Ye *et al.* (18) found that increased creatine kinase and decreased blood platelet count are useful in assessing the progression of HS, thereby enabling timely prediction of complications. Zhao *et al.* (19) reported that disseminated intravascular coagulation (DIC) and AKI are the only two significant prognostic factors for HS among all its complications, including MODS, that predict increased HS-related mortality. Another study demonstrated that AKI occurred during the early stages of HS and lasted for a sustained period of time, before progressing to ARF if left untreated (20). Moreover, a study also found that occurrence of AKI has been associated with increased myeloperoxidase, tumor necrosis factor- α and interleukin-6 levels in the kidneys (21). A study on *CASQ1*-knockout mice indicated that calsequestrin-1 could be a novel candidate gene for malignant hyperthermia and EHS (22). Unfortunately, the identification of all of these parameters associated with HS has resulted in only limited improvements in the treatment of HS. Therefore, understanding the potential mechanisms underlying HS is important for improving the treatment of HS.

Several mechanisms involved in HS are currently accepted. Systemic inflammation and MODS are reported to play key roles in the pathophysiology of HS (23,24). HS causes dysfunction of the intestinal barrier (25), leading to intercellular penetration of harmful substances such as bacteria and endotoxins within the gut lumen. The bacteria and endotoxins then seep into the circulation, and cause inflammation and cytokine secretion, which will eventually result in systemic inflammatory response syndrome (SIRS) and MODS (26,27). Metabolomics profiling, an emerging research methodology of systems biology, enables the comprehensive and quantitative analysis of all metabolites in a biological sample and the identification of their direct associations with biological phenotypes, such as responses to a disease or a drug treatment or intervention (28,29). In contrast to genomics and proteomics, which focus on intermediate media, metabolomics measures end products, which helps in accurate identification of disease pathogenesis. HS increases glucose utilization, which reduces the availability of the metabolic substrates required for proper function of the brain, heart and muscles (30).

In the present study, a mouse model of HS was constructed to examine whether the high-mobility group box 1 (HMGB1)/receptor for advanced glycosylation end products (RAGE) pathway is activated in mouse kidneys.

Metabolomics analysis was performed to investigate the underlying mechanisms of HS. A total of 136 differential metabolites were screened out and analyzed, and several important signaling pathways that may play important roles in HS development, including 'biosynthesis of unsaturated fatty acids', were determined to be enriched.

Materials and methods

Animals. The present study was conducted on 20 8-week-old male C57BL/6J mice (weight, 21-23 g; Beijing HFK Bioscience Co., Ltd.). The mice were housed in a specific pathogen-free and 40-50% humidity environment at the animal laboratory of the Affiliated Hospital of Southwest Medical University (free access to food and water; 12-h light/12-h dark cycle; 24°C). All animal experiments complied with the guidelines of the Animal Care and Use Committee of the Southwest Medical University; the study protocol was approved by the same committee.

Experimental design. The mice were randomly divided into control (no heat exposure) and HS groups (heat exposure). The experimental design was based on a previously described method (31-33). After being subjected to 6 h of fasting, the HS group was housed in a temperature-controlled environment at 41.0°C (relative humidity, 60%). An infrared thermometer (MC818A; Shenzhen MileSee Technology Co., Ltd.) was used to detect the shell temperature of the mice every 15 min until the temperature reached 41°C. Electrodes were then inserted into the rectum of each mouse to re-detect the temperature. The onset of HS was defined as when the core temperature exceeded 41°C (34). In the experimental group, all mice were immediately withdrawn from the heat environment and showered with cold water to rapidly decrease their core temperature to 37.0°C. This temperature was maintained by placing the mice in ambient conditions (26°C). In the control group, the core temperature of the mice was maintained at 36°C using a folded heating pad, if needed. Control animals were housed in the same temperature-controlled environment at the HS group during the protocol. After model construction, two mice from each group were selected for a micro-positron emission tomography-computed tomography (micro-PET/CT) scan. All mice were then anesthetized with 3% pentobarbital sodium (30 mg/kg) by intraperitoneal injection and sacrificed via cervical dislocation. Death was ascertained based on pupil dilation and an inability to palpate the carotid pulse. Blood samples were then collected, and the kidneys were dissected and fixed in 4% paraformaldehyde for 30 min at room temperature for follow-up examinations.

Plasma glucose and creatinine levels. Before sacrificing the mice, peripheral plasma glucose levels were measured with a blood glucose meter (Roche Applied Science). The tails were removed to ensure that ^{18}F -deoxyglucose (^{18}F FDG), which was injected into the tail vein for micro-PET/CT, did not influence the peripheral plasma glucose level measurements. Cardiac blood samples were collected immediately after cervical dislocation. Subsequently, peripheral and cardiac blood was centrifuged at 2,000 \times g for 30 min at room temperature to isolate the plasma, which was stored at -80°C. The obtained

plasma was then transported to a diagnostic laboratory for the measurement of creatinine levels using an Indiko™ system (Thermo Fisher Scientific, Inc.).

Micro-PET/CT scanning. ¹⁸F-DG is a commonly used radio-nuclide imaging agent that is actively absorbed by cells as an energy substrate and indirectly reflects the energy metabolism of the body. ¹⁸F-DG (3.7 MBq/kg), obtained from an Eclipse HP/RD accelerator (Siemens AG), was injected into the tail vein 20 min before the scan. The radioisotope uptake of the tissues, which reflects the status of the body's energy metabolism, was detected using an Inveon™ micro-PET/CT system (Siemens AG). The test parameters were set as follows: Resolution of transverse, longitudinal and axial directions of the PET module, 1.5 mm; collection timing window, 3.4 nsec; energy window, 350-650 keV; and collection time, 10 min. The filtered back projection algorithm was used for reconstruction. The images were analyzed using Inveon image acquisition (IAW 1.5; Siemens AG). The PET value was set at 1.8-9.9, and the CT window width at 500-1000 HU.

H&E staining. Paraformaldehyde-fixed kidney tissues were paraffin-embedded, cut into 4- μ m sections, deparaffinized, and serially rehydrated using xylene, an ethanol gradient series (100, 96, 80 and 70% ethanol) and finally H₂O. Next, the sections were stained with 10% hematoxylin for 5 min at room temperature (Sigma-Aldrich; Merck KGaA), washed, stained with 1% eosin (Sigma-Aldrich; Merck KGaA) supplemented with 0.2% glacial acetic acid for 5 mins at room temperature, immediately washed again, and dehydrated using an ethanol gradient (70, 80, 96 and 100%) and xylene. Finally, the sections were examined under an inverted phase-contrast microscope (DMI1; Leica Microsystems GmbH). The renal tubule injury score based on the Parller system was calculated to analyze renal injury (35). A total of 10 renal tubules within 10 non-overlapping high magnification fields were randomly selected for a total of 100 renal tubules, which were then evaluated to determine the renal tubule injury score as follows: Normal structure of the epithelial cells, 0 points; obvious renal tubule expansion, loss of brush border, epithelial cell edema, vacuolar degeneration, granular degeneration and/or nuclear deflation, 1 point; and foaming of the cell membrane, cell necrosis and/or tubular appearance in the tubule lumen, 2 points. The sum of the scores for all 100 tubules was used as the Parller score for each animal.

Immunohistochemistry (IHC) analysis. In brief, 4- μ m paraffin-embedded sections were deparaffinized, subjected to antigen retrieval using citrate buffer (pH 6.0) at 95°C for 10 min and treated with 0.3% H₂O₂ to block their endogenous peroxidase activity at room temperature for 10 min. Next, the sections were continuously treated with blocking reagent QuickBlock™ (cat. no. P0260; Beyotime Institute of Biotechnology), then incubated with the appropriate primary antibodies, such as apoptosis-inducing factor mitochondria-associated 2 (Aifm2; 1:1,000; cat. no. GXP20453; GenXspan) and HMGB1 (1:100; cat. no. ab227168; Abcam) at 4°C overnight, and then with the secondary antibody (1:5,000; cat. no. TA130017 Biotinylated Goat anti rabbit; OriGene Technologies, Inc.) for 1 h at room temperature. Peroxidase

activity was visualized using 3,3'-diaminobenzidine at room temperature for 5 min. The relative expression density and location of Aifm2 and HMGB1 in the mouse kidney tissues were quantified at x400 magnification per 30 fields, according to the Envision method (36), by two pathologists blinded to the experiment. The relative expression of proteins located mainly in the cytoplasm was calculated using the relative mean absorbance according to the Envision method. The relative expression of proteins located mainly in the nucleus was determined as the number of positive cells per 200 cells in a high-power field (magnification, x400). All IHC sections were examined with a phase-contrast microscope. Image-Pro Plus 6 software (Media Cybernetics, Inc.) was used for analysis.

Transmission electron microscopy (TEM). Dissected mouse kidneys were fixed in 2.5% glutaraldehyde at 4°C overnight, washed three times with 0.1 M PBS and stained with 1% osmium acid at 4°C for 3 h. The sections were then washed 3 times with PBS, dehydrated in ethanol and subsequently propylene oxide, embedded in Spurr resin at room temperature overnight and finally polymerized at 70°C overnight. The embedded sections were cut into 70-nm slices. Slides of these slices were prepared and stained with lead citrate and uranium dioxide acetate at 80°C for 15 min, and photographed under a transmission electron microscope.

TUNEL assay. Sections (2-3 μ m) of mouse kidney tissues were incubated for 2 min with 0.1% Triton X-100 and washed using ice-cold PBS. Cell apoptosis was assayed using TUNEL reagent for 60 min at 37°C (Roche Applied Science), according to the manufacturer's protocols. Cells with yellow-stained nuclei were defined as positive cells at 25°C for 10 min (Concentrated DAB reagent kit; OriGene Technologies, Inc.). The positive cells in 200 randomly selected cells were counted using a phase-contrast microscope (magnification, x100; 10 fields of view).

Western blot analysis. The dissected kidney tissues were lysed and sonicated (20 sec per 5 min) for 30 min on ice in radioimmunoprecipitation assay buffer (Beyotime Institute of Biotechnology) supplemented with a protease inhibitor and a phosphatase inhibitor (Sigma-Aldrich; Merck KGaA) on an ice bath for 30 min. The tissues were then centrifuged for 15 min at 13,000 x g and 4°C. The supernatant thus obtained was subjected to the bicinchoninic acid assay for protein quantitation, and bovine serum albumin (Beyotime Institute of Biotechnology) was used as the standard. In brief, 40 μ g protein extracts were denatured, separated via 10% SDS-PAGE, and transferred to Hybond® polyvinylidene difluoride membranes. The membranes were washed and blocked using 0.1% TBS-Tween buffer and 5% non-fat milk (BD Biosciences) at room temperature for 2 h and subsequently probed with RAGE (1:2,000; cat. no. ab3611; Abcam), HMGB1 (1:2,000; cat. no. ab227168; Abcam) and β -actin (1:5,000; cat. no. ab8226; Abcam) primary antibodies at 4°C overnight, and secondary antibodies for 1 h at room temperature [1:5,000; Biotinylated Goat anti rabbit IgG (H + L); cat. no. ab6721; Abcam] Protein bands were evaluated using enhanced chemiluminescence reagent (Bio-Rad Laboratories, Inc.) and Biomax MR films (Kodak). Relative

protein abundance of the indicated proteins was determined using ChemiDoc XRS+ System/Image Lab Software version 2.0 (Bio-Rad Laboratories, Inc.).

Liquid chromatography-mass spectrometry (LC-MS) analysis. All chemicals and solvents used were of analytical or high-performance liquid chromatography grade. Acetonitrile, formic acid, methanol and water were acquired from CNW Technologies GmbH, and 2-chloro-L-phenylalanine from Shanghai Hengchuang Bio-technology Co., Ltd. Aliquots of the samples (30 mg) were transferred to tubes containing two small steel balls. To each tube, 400 μ l extraction solvent with methanol water (4:1, v/v) and 20 μ l internal standard (2-chloro-L-phenylalanine in methanol, 0.3 mg/ml) were added. The samples were frozen to -80°C for 2 min, ground for 2 min at 60 Hz, ultrasonicated (frequency, 40 KHz; capacity, 200 W) for 10 min in ice water bath, and frozen again to -20°C for 20 min. The extract was centrifuged for 10 min at $15,624 \times g$ in 4°C . Supernatants (200 μ l) from each tube were collected using crystal syringes, filtered using microfilters (pore size, 0.22 μm) and transferred to liquid chromatography vials. The vials were stored at -80°C until LC-MS analysis.

An ACQUITY UPLC BEH C18 column (1.7 μm , 2.1x100 mm) was employed in both positive and negative modes. The binary gradient elution system consisted of (A) water (containing 0.1% formic acid, v/v) and (B) acetonitrile (containing 0.1% formic acid, v/v) and separation was achieved using the following gradient: 0 min, 5% B; 2 min, 20% B; 4 min, 25% B; 9 min, 60% B; 14 min, 100% B; 18 min, 100% B; 18.1 min, 5% B and 19.5 min, 5% B. The flow rate was 0.4 ml/min and the column temperature was 45°C . All the samples were kept at 4°C during the analysis. The injection volume was 5 μ l. Data acquisition was performed in full scan mode (m/z; ranges from 70-1,000 m/z) combined with IDA mode. Parameters of mass spectrometry were as follows: Ion source temperature, 550°C (+) and 550°C (-); ion spray voltage, 5,500 V (+) and 4,500 V (-); curtain gas of 35 PSI; declustering potential, 100 V (+) and -100 V (-); collision energy, 10 eV (+) and -10 eV (-); and interface heater temperature, 550°C (+) and 600°C (-). For IDA analysis, range of m/z was set as 25-1,000 m/z, the collision energy was 30 eV. The QCs were injected at regular intervals (every 10 samples) throughout the analytical run to provide a set of data from which repeatability can be assessed. Metabolic profiles were analyzed in both the electrospray ionization-positive and electrospray ionization-negative modes by using an AB SCIEX Triple TOF 5600 system (SCIEX) and an ACQUITY UHPLC system (Waters Corporation).

Identification of differential metabolites. The raw data obtained from LC-MS were analyzed using Progenesis QI (v 2.3; Waters Corporation) for baseline filtering, peak identification and alignment, normalization, integration and retention time correction. Quantitative analysis was performed using the Metlin metabolite database (metlin.scripps.edu), the Human Metabolome Database (<http://www.hmdb.ca/>) and LIPID MAPS (<http://www.lipidmaps.org/>). The metabolic alterations in each group were visualized using orthogonal partial least squares discriminant analysis (OPLS-DA) and principal component analysis (PCA). Differential metabolites

Table I. Change in blood glucose and creatinine levels in the study groups.

Group	Glucose, mmol/l	Serum creatinine, $\mu\text{mol/l}$
Control	5.26 \pm 1.63	11.47 \pm 3.91
Heat stroke	5.34 \pm 1.92	20.53 \pm 4.75 ^a

^aP<0.05 Heat stroke vs. Control.

were defined as metabolites with variable influence on projection values >1.0 (obtained using the OPLS-DA model) and P<0.05 (obtained using a two-tailed Student's t-test of normalized peak areas).

Pearson correlation coefficient analysis was used to calculate the correlations among the differential metabolites. Moreover, MBRole 2.0 (37) pathway analysis of the differential metabolites was conducted using the Kyoto Encyclopedia of Genes and Genomes (KEGG) database (38) to determine signaling pathways associated with HS-related AKI.

Statistical analysis. All statistical analyses were performed using SPSS v22.0 (IBM Corp.). Measurement data are expressed as the mean \pm SD. Between-group comparisons were performed using unpaired Student's t-test. The heat map and volcano plot were performed and analyzed using 'pheatmap' packages in R 3.5.3. P<0.05 was considered to indicate a statistically significant difference.

Results

HS can induce SIRS. After inducing HS in mice, ^{18}F FDG was injected into the tail vein of each of the 4 mice selected for the measurement of changes in energy metabolism. As ^{18}F FDG is a glucose analog that influences cell metabolism by inhibiting glycolysis, peripheral plasma glucose levels were analyzed. The results indicated that there were no significant differences in plasma glucose concentrations between the control group (5.1 and 5.4 mM) and the HS group (5.2 and 5.5 mM; Table I). Micro-PET/CT showed that in the control group, the uptake and dispersion of the radionuclide imaging agent occurred only in the skeletal muscles and brain, which are metabolically active organs (Fig. 1A). In the HS model, the intestine was diversely metabolically activated, and the integrity of the intestinal barrier may be disrupted, as indicated by the accumulation of the imaging agent in the intestinal barrier, which led to the release of bacteria and endotoxins into the circulation, influencing the whole body. The radionuclide imaging agent had also accumulated in the liver, brain, and kidneys, indicating the presence of SIRS and MODS. Moreover, it was noted that in the HS group, the kidneys were more active than the other organs (Fig. 1B).

HS triggers AKI in mice. The plasma creatinine level was significantly upregulated in the HS group compared with the control group (P<0.05; Table I). In the HS group, H&E staining revealed glomerular swelling, inflammatory cell infiltration, vacuolar degeneration of endothelial cells and red blood cells in renal tubules, which is a characteristic sign of hyperemia and

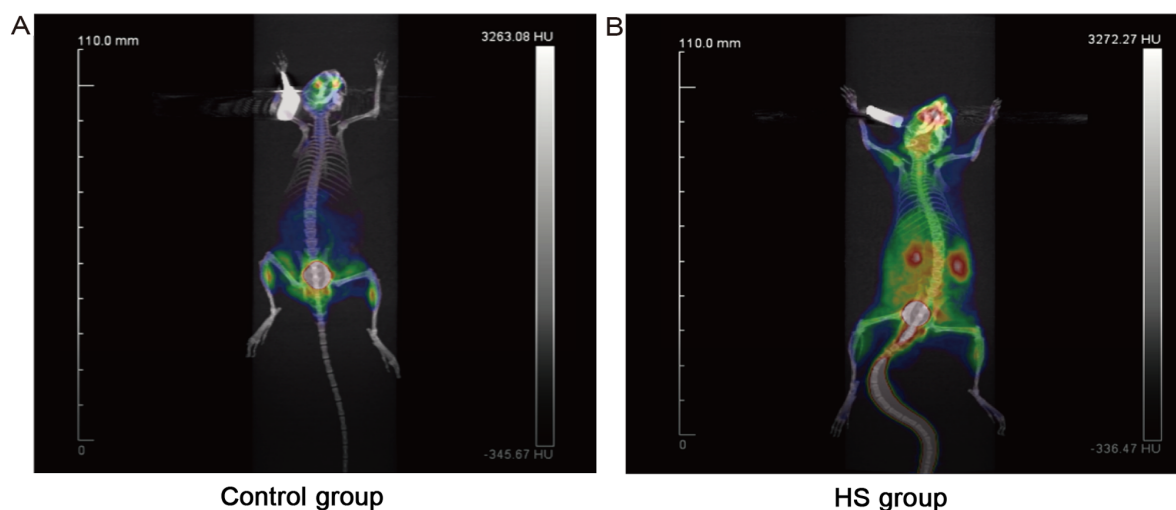


Figure 1. ^{18}F -FDG-labeled micro-PET/CT scanning. Mice were injected with ^{18}F -FDG and subjected to micro-PET/CT to visualize energy metabolism. (A) Control group (n=2). (B) HS group (n=2). Red indicates high uptake and dispersion of the radionuclide imaging agent, whereas green indicates low uptake and dispersion of the radionuclide imaging agent. HS, heat stroke; micro-PET/CT, micro-positron emission tomography-computed tomography; ^{18}F -FDG, ^{18}F -deoxyglucose.

indicates a high risk of hemorrhage (Fig. 2C and D). All these changes were not present in the control group (Fig. 2A and B). The TUNEL assay revealed yellow-stained nuclei of apoptotic cells primarily located in the renal tubule area in the HS group. The number of apoptotic cells was significantly increased in the HS group compared with in the control group ($P < 0.05$; Fig. 2E, F and M). Moreover, the renal tubule injury score was significantly increased in the HS group compared with in the control group ($P < 0.001$; Fig. 2N). TEM revealed swollen mitochondria with diminished inner ridges in the HS group (Fig. 2G-L). All of these changes indicated HS-induced AKI.

HS activates the HMGB1/RAGE pathway. IHC staining revealed cytoplasmic expression of Aifm2 in the kidney tissues in both groups, but the expression was significantly increased in the HS group compared with in the control group ($P < 0.05$; Fig. 3A-B). HMGB1 was primarily expressed in the nuclei of the renal tubule cells in both groups; however, HMGB1-positive cells were abundant in the HS group and rarely observed in the control group ($P < 0.05$; Fig. 3C and D). Western blot analysis revealed that the expression levels of HMGB1 and RAGE were significantly elevated in the HS group compared with in the control group ($P < 0.05$; Fig. 3E and F).

Metabolomic evaluation of HS model. Intrinsic clustering and potential outliers were detected using PCA. A plot of PC1 vs. PC2 scores ($R^2_X = 0.691$, $Q^2 = 0.528$; Fig. 4A and B) showed good separation between the control and HS groups, except for three outliers. PLS-DA also showed good separation in the scatter plot ($R^2_X = 0.794$, $R^2_Y = 0.736$, $Q^2 = 0.472$; Fig. 4C). To minimize any potential effects of intergroup variability and improve the between-group separation, the OPLS-DA scores were plotted (Fig. 4D) through LC-MS analysis of the kidney tissues, and a distinct separation between the HS and control groups was found ($R^2_X = 0.794$, $R^2_Y = 0.736$, $Q^2 = 0.006$), which demonstrated a difference in kidney metabolites between the two groups. The OPLS-DA model was selected for the following experiment to examine variations in metabolite profiles between the groups.

Identification of differential metabolites and signaling pathways. OPLS-DA models were used to identify differences in metabolites between the control and HS groups. The HS-group cluster was distant from the control-group cluster (Fig. 4). The results revealed that of the 136 metabolites that were differentially expressed in the HS and control groups, 80 were upregulated and 56 were downregulated (Fig. 5A and Table SI). The top 50 metabolites were selected to construct a heat map, and it was found that the differential metabolites were highly efficiently clustered in each group (Fig. 5B). A majority of the differential metabolites exhibited high correlation with other different metabolites (Fig. 6A). These results indicated that the screened-out metabolites may cooperate with each other to induce AKI in response to HS. To further investigate the mechanism of AKI in HS, enrichment analysis was performed using the KEGG pathway database. The results revealed that the 'biosynthesis of unsaturated fatty acids', 'synthesis and degradation of ketone bodies', 'Chagas disease', 'D-arginine and D-ornithine metabolism' and 'amyotrophic lateral sclerosis (ALS)' pathways were the only five signaling pathways significantly enriched with differential metabolites (Fig. 6B). Adrenic acid, docosahexaenoic acid (DHA), eicosa-pentaenoic acid (EPA), stearic acid, acetone and L-arginine were the metabolites enriched in these signaling pathways.

Discussion

Recently, an increasing number of studies (39-41) focusing on high temperature-related diseases have been published, primarily due to the continuously and rapidly increasing HS-related morbidity and mortality rates (23). In addition to affecting the temperature-regulation system, HS can cause several complications, such as rhabdomyolysis, ARF, acute respiratory distress syndrome, hepatic failure and DIC, all of which can eventually progress to MODS, which commonly results in mortality for affected individuals (42).

HS is considered to be to an SIRS-like disease that is triggered by endotoxins, cytokines and other immune-regulatory factors (43). Impaired integrity of the intestinal barrier and

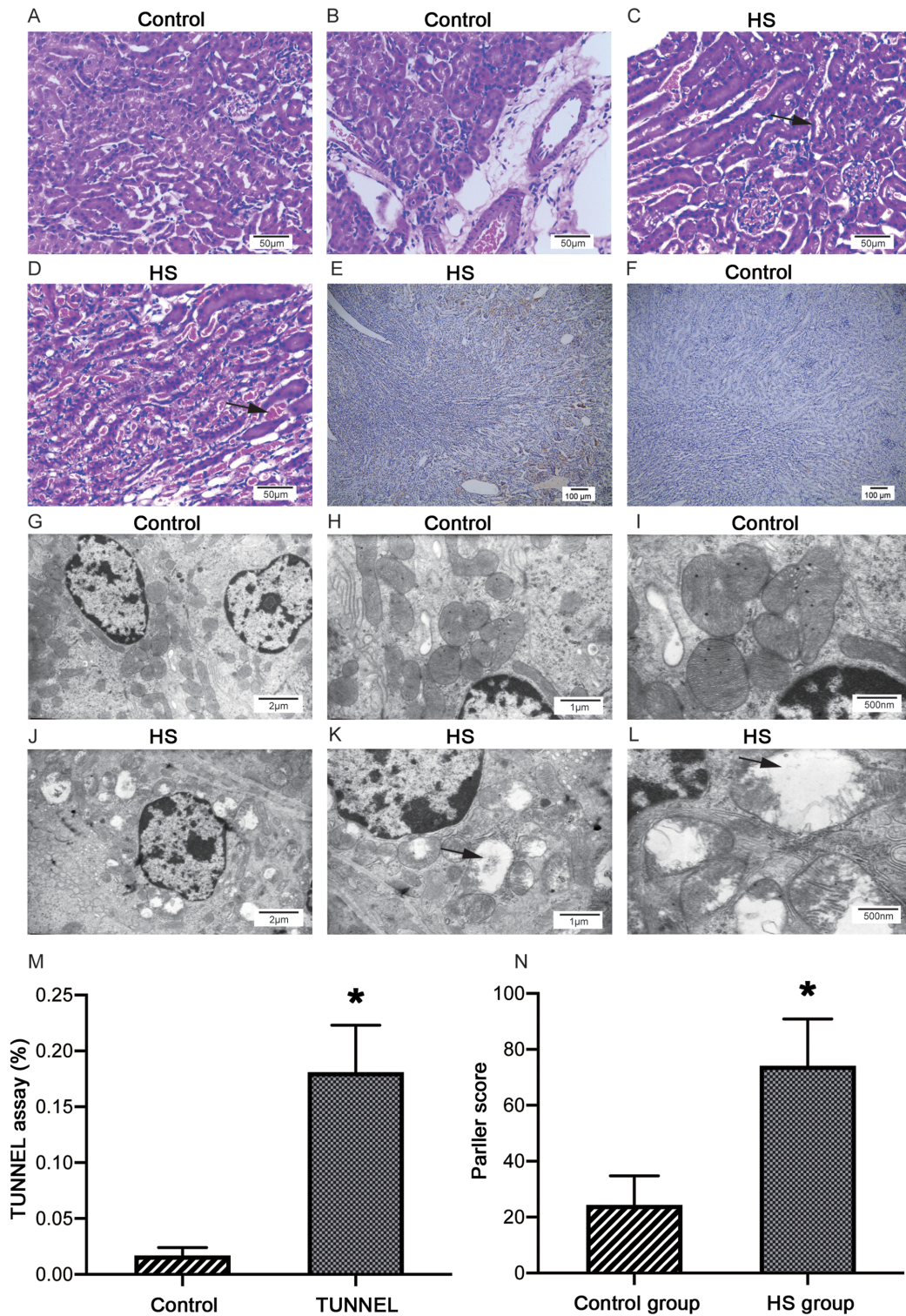


Figure 2. HS triggers acute kidney injury in mice. (A-D) Representative H&E-stained images of the kidneys in both groups. HS group (n=8) displays glomerular swelling, inflammatory cell infiltration, vacuolar degeneration of endothelial cells and red blood cells in the renal tubules (C and D). These changes were not found in the control group (n=8) (A and B). Scale bar, 50 μ m. Representative TUNEL assay images of the kidneys in the (E) HS (n=8) and (F) control groups (n=8). Yellow nuclear staining indicates apoptotic cells in the kidney tissues. scale bar, 100 μ m. Representative transmission electron microscope images of the kidneys in the (G-I) control (n=8) and (J-L) HS group (n=8). Scale bar, 2 μ m in G and J, 1 μ m in H and K, and 500 nm in I and L. (M) Statistical analysis of the TUNEL assay. * P <0.05 HS group (n=8) vs. Control group (n=8). (N) Statistical analysis of renal tubule injury in the HS (n=8) and control groups (n=8). * P <0.05 HS group vs. Control group. HS, heat stroke.

increased intestinal permeability may be the cause of these factors entering the circulation, as was reported by a study, which revealed increased leakage of lipopolysaccharides (LPS) and endotoxins into the circulation from the gut during

HS (44,45). Furthermore, another study found that the use of anti-LPS antibodies can prevent this translocation during HS (46). Translocation of endotoxins and LPS induces the release of various cytokines and HMGB1, a prototypic alarmin,

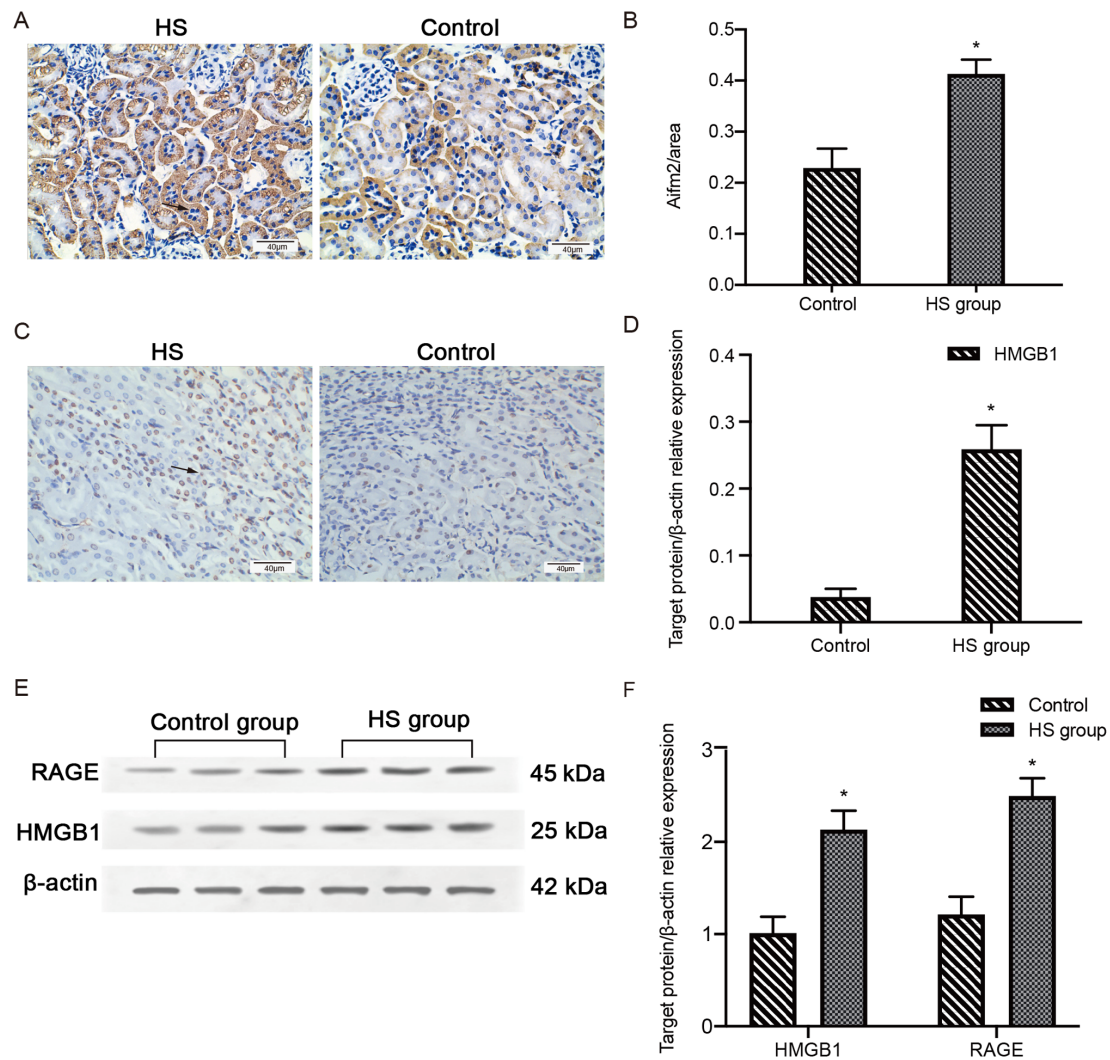


Figure 3. HS activates the HMGB1/RAGE pathway. (A) Representative IHC staining of Aifm2 protein expression in the kidneys of HS (n=5) and control group (n=5) mice. Aifm2 is mainly located in the cytoplasm of kidney tissues. Scale bar, 40 μ m. (B) Statistical analysis of the IHC staining of Aifm2. *P<0.05 HS (n=5) vs. Control (n=5) group. (C) Representative IHC staining of HMGB1 protein expression in the dissected kidneys of HS (n=5) and Control (n=5) group mice. HMGB1 is mainly located in the nuclei of kidney tissues. Scale bar, 40 μ m. (D) Statistical analysis of the IHC staining of HMGB1. *P<0.05 HS (n=5) vs. Control (n=5) group. (E) Western blot analysis of HMGB1 and RAGE in kidney tissues. (F) Relative protein abundance of the indicated proteins determined using Quantity One. *P<0.05 HS (n=8) vs. Control (n=8) group. HS, heat stroke; IHC, immunohistochemistry; Aifm2, apoptosis-inducing factor mitochondria-associated 2; HMGB1, high-mobility group box 1; RAGE, receptor for advanced glycosylation end products.

which causes excessive activation of leukocytes and endothelial cells, resulting in the development of SIRS (47,48). Therefore, protecting the integrity of the intestinal barrier appears to be important for preventing HS. Furthermore, the combination of inflammatory factors and direct cytotoxic effects of heat may cause injury to the vascular endothelium, resulting in microthromboses (49). Certain authors have reported significantly different expression of long non-coding RNAs and their competing endogenous RNAs in exosomes secreted from human umbilical vein endothelial cells in response to HS (50). Although these studies may identify certain biomarkers involved in HS, the function and regulatory mechanisms underlying the condition remain unexplored (50). In HS, microthrombosis-induced platelet consumption and hyperthermia-induced platelet aggregation both lead to a decreased platelet count (51). Although thrombocytopenia has been associated with the development and prognosis of AKI in HS (52), the precise mechanism underlying AKI in HS remains unclear.

In the present study, a mouse model of HS was established. Heat stress led to an increase in plasma creatinine levels in the HS group compared with the control group. This demonstrated that the renal function of heat-stressed mice was impaired, and this deficiency in the HS mice may be comparable to AKI. Micro-PET/CT scanning was used to visualize the uptake and dispersion of 18 F 18 FDG in mice. The tissue uptake of 18 F 18 FDG is highly increased during states of inflammation and hypercatabolism (53). Although a glucose analog, 18 F 18 FDG did not influence blood glucose concentrations in the present study, indicating that it has no role in mouse glucose metabolism. 18 F 18 FDG accumulation was noted in all organs, including the liver, intestine and kidneys, in the HS group, which indicated that HS may induce SIRS in mice. It was also found that 18 F 18 FDG was primarily aggregated in the kidneys, which is consistent with the increase observed in the creatinine levels of the mice. Earlier studies have investigated the pathogenesis of HS mainly in terms of systemic inflammation (54) or nervous system protection (55).

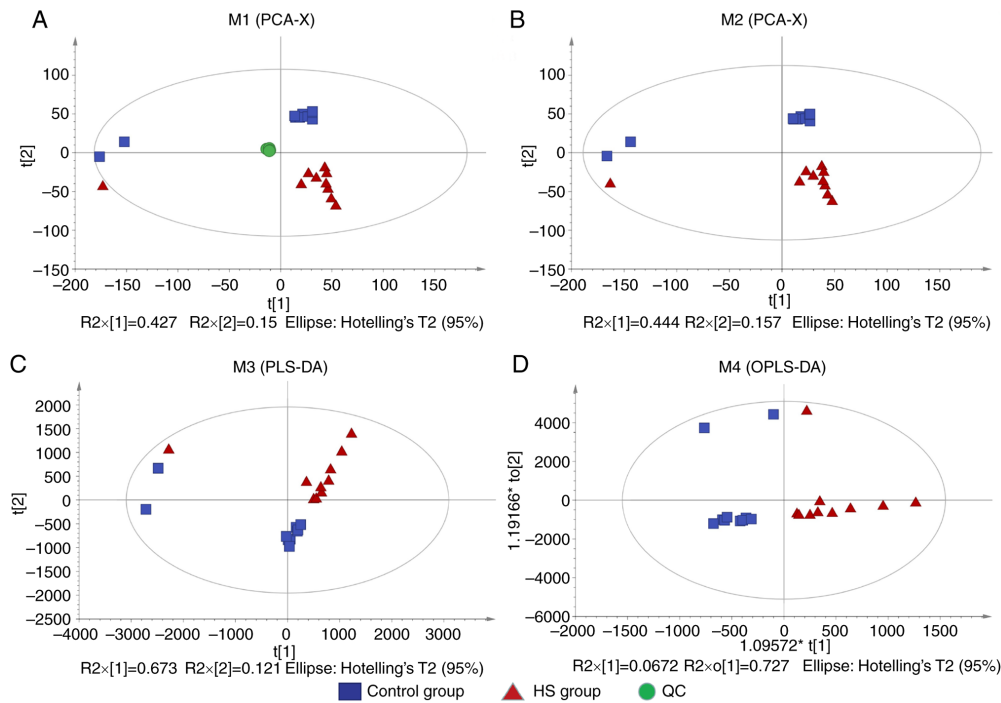


Figure 4. Scatter plots of scores established by PCA. (A) Multivariate statistical comparison of PCA between the two groups with quality control. (B) Multivariate statistical comparison of PCA between the two groups without quality control. (C) PLS-DA. (D) OPLS-DA. PCA, principal component analysis; OPLS-DA, orthogonal partial least squares discriminant analysis; PLS-DA, partial least squares discriminant analysis; HS, heat stroke; QC, quality control.

The present study aimed to acquire a deeper understanding of the mechanisms underlying HS-induced AKI, which has been rarely studied and could provide novel insight.

HMGB1, also known as alarmin, is a gene transcription cofactor and a damage-associated molecular pattern molecule that mediates proinflammatory effects by activating multiple cell surface receptors, such as RAGE and Toll-like receptors (56). This proinflammatory role is relevant to the pathogenesis of several kidney diseases, including AKI (57). HMGB1 is also considered to be involved in the pathogenesis of HS, as increased serum HMGB1 levels indicate poor prognosis in HS (48). Inhibiting the HMGB1/RAGE pathway may aid in the treatment of AKI, although its role in HS-related AKI is unclear (58). It was observed that both HMGB1 and RAGE were significantly upregulated in the kidneys of HS mice. Furthermore, both the TUNEL assay and TEM scanning suggested that mitochondrial-dependent apoptosis had occurred in the kidneys of HS mice, which was supported by the upregulation of Aifm2, a gene involved in mitochondrial-dependent apoptosis (59). As the HMGB1/RAGE pathway may trigger mitochondria-related apoptosis in inflammatory states (60), it is hypothesized that the apparent increase in renal tubular epithelial cell apoptosis observed in the present study was caused, at least partly, by the HMGB1/RAGE pathway. However, pathological examination indicated renal tubular hyperemia and edema, instead of apoptosis. A previous study has reported the occurrence of severe pulmonary hemorrhage in patients who died of HS; however, kidney injury due to HS was not mentioned (61). Hence, it is proposed that bleeding, rather than apoptosis, may be a characteristic feature of HS-associated AKI. Moreover, HS-induced SIRS and secondary hyperfibrinolysis may be other reasons for hyperemia and edema in the kidneys, which were different from the reported manifestations of common acute tubular necrosis (23). Dysregulation of the

HMGB1/RAGE pathway may be involved in this process (62), but the specific mechanism needs to be elucidated.

In present study, metabolomics analysis of the animal model was conducted to further explore the pathogenesis of HS. Of the 136 differential metabolites, 80 metabolites were upregulated and 56 were downregulated. The top 15 differential metabolites were associated with fatty acid metabolism and other associated metabolic pathways, which may induce early changes in the kidneys during HS. Additionally, the correlation among a number of the top 50 metabolites was strong, indicating their probable interplay in inducing AKI in response to HS. Enrichment analysis of all the differential metabolites was performed, and 'biosynthesis of unsaturated fatty acids', 'synthesis and degradation of ketone bodies', 'Chagas disease', 'D-arginine and D-ornithine metabolism' and 'ALS' were the only five significantly enriched signaling pathways between the two groups. Adrenic acid, DHA and EPA, which are involved in the 'biosynthesis of unsaturated fatty acids' pathway, were upregulated in the HS group. This may appear to be in contrast to a previous study, which reported the synergistic functioning of DHA and EPA to protect intestinal barrier integrity in HS (63). However, these are, in fact, two phases of a process. HS can damage the intestine barrier to allow the seepage of unsaturated fatty acids, which are important components of cell membranes, into the urinary system, leading to an increase in their levels in the urinary system. As DHA and EPA treatment prevents the disruption of the intestinal barrier, fewer metabolites, such as unsaturated fatty acids, flow into the circulation to initiate inflammatory processes, and the damage caused by HS is limited. As reported previously, the HMGB1/RAGE pathway may be a potential target for unsaturated fatty acids or regulate the concentration of unsaturated fatty acids in other diseases via

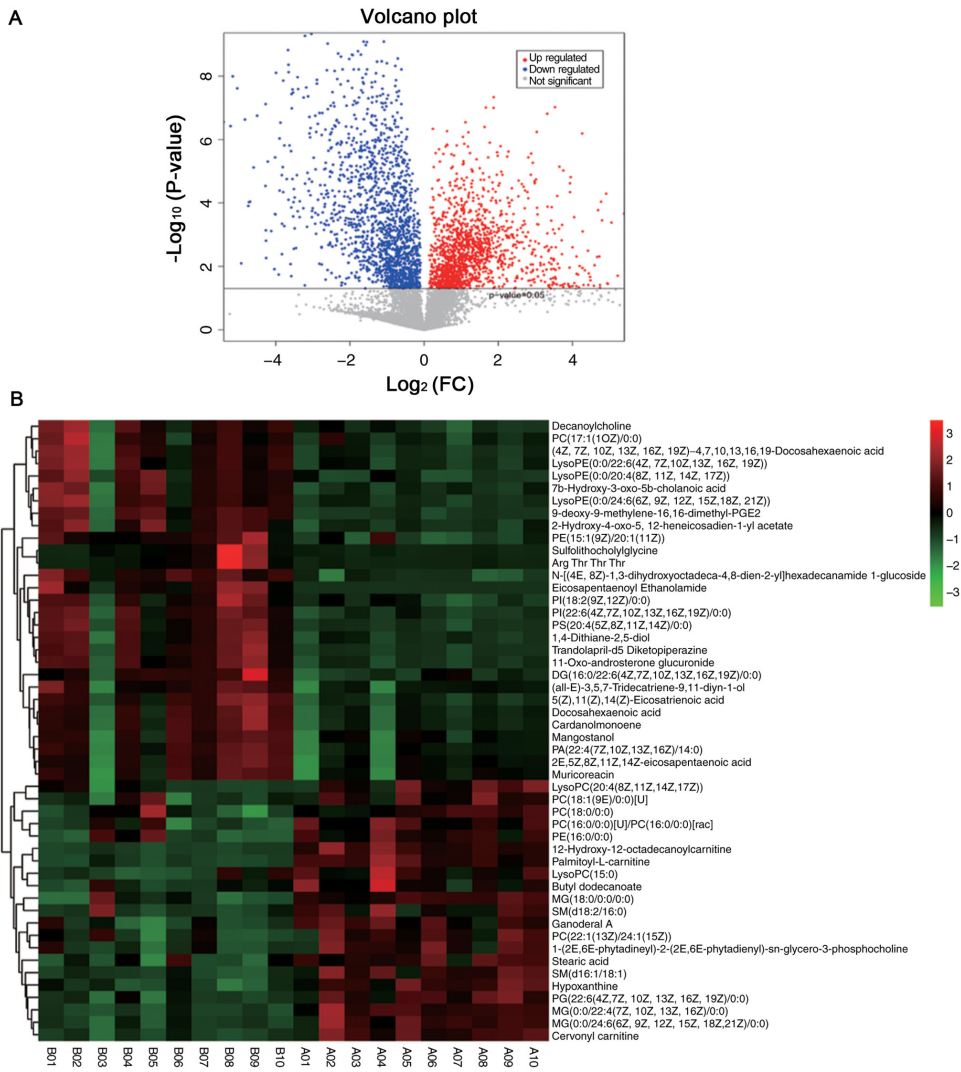


Figure 5. Identification of differential metabolites. (A) Volcano plot of the total metabolites. Red indicates upregulated metabolites, and blue indicates downregulated metabolites. (B) Heat map of the top 50 differential metabolites in the heat stroke group (A1-10) compared with the control group (B1-10). Red indicates upregulated metabolites, and green indicates downregulated metabolites. FC, fold change.

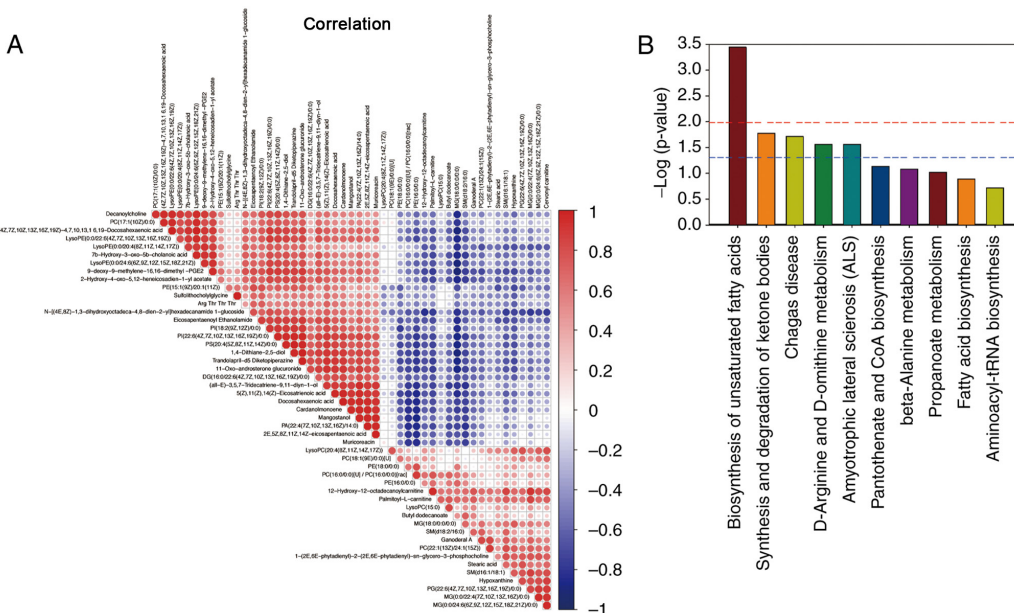


Figure 6. Identification of enriched signaling pathways. (A) Correlation analysis of top 50 differential metabolites. Red indicates positive correlation, and blue indicates negative correlation. (B) Histogram of top 10 significantly enriched signaling pathways between the two groups.

various means (64,65). At present, the relationship between the HMGB1/RAGE pathway and unsaturated fatty acids remains unclear, and further studies are required.

The present study has certain limitations. First, for a more in-depth investigation of the mechanisms underlying HS-related AKI, multiple observation time points should be used, such as 15 and 30 min, and 1 and 2 h; this will be explored in subsequent studies. Second, the correlations between metabolic changes and alterations in signaling pathways should be verified using gain-or-loss experiments. Third, as HS is a complex disease that involves alterations in diverse signaling pathways, therapeutic interventions targeting the HMGB1/RAGE pathway or biosynthesis of unsaturated fatty acids could be added in future studies into HS.

In summary, the present study suggested that HS-associated AKI is the most common result of HS-induced SIRS, and may be associated with the HMGB1/RAGE pathway. Furthermore, a feedback loop between the HMGB1/RAGE pathway and the biosynthesis of unsaturated fatty acids may contribute to the progression of HS-related AKI. Therefore, it is of great importance to elucidate the relationship between the HMGB1/RAGE pathway and disordered unsaturated fatty acid metabolism in the pathogenesis of HS-associated AKI.

Acknowledgements

Not applicable.

Funding

The study was supported by National Natural Science Foundation of China (grant no. 81200533), Sichuan Clinical Research Center for Nephropathy (grant no. 2019YFS0537-4) and Luzhou Municipal Government-Southwest Medical University Strategic Cooperation Fund (grant no. 2016LZXNYD-J20).

Availability of data and materials

The datasets used and/or analyzed during the current study are available from the corresponding author on reasonable request.

Authors' contributions

LX and WW designed the study and participated in animal experiments. LX and WG participated in the study design and drafting the manuscript. LL and SO were responsible for statistical analysis of the metabolomic data. TZ performed *in vivo* animal experiments. LC and WD performed PET/CT scanning and data analysis. All authors read and approved the final manuscript.

Ethics approval and consent to participate

All animal experiments complied with the guidelines of the Animal Care and Use Committee of the Southwest Medical University. The study protocol was approved by the same committee.

Patient consent for publication

Not applicable.

Competing interests

The authors declare that they have no competing interests.

References

- Laitano O, Murray KO and Leon LR: Overlapping mechanisms of exertional heat stroke and malignant hyperthermia: Evidence vs. conjecture. *Sports Med* 50: 1581-1592, 2020.
- Gaudio FG and Grissom CK: Cooling methods in heat stroke. *J Emerg Med* 50: 607-616, 2016.
- Barriopedro D, Fischer EM, Luterbacher J, Trigo RM and Garcia-Herrera R: The hot summer of 2010: Redrawing the temperature record map of Europe. *Science* 332: 220-224, 2011.
- Kovats RS and Kristie LE: Heatwaves and public health in Europe. *Eur J Public Health* 16: 592-599, 2006.
- Argaud L, Ferry T, Le QH, Marfisi A, Ciorba D, Achache P, Ducluzeau R and Robert D: Short- and long-term outcomes of heatstroke following the 2003 heat wave in Lyon, France. *Arch Intern Med* 167: 2177-2183, 2007.
- Roux-Buisson N, Monnier N, Sagui E, Abriat A, Brosset C, Bendahan D, Kozak-Ribbens G, Gazzola S, Quesada JL, Foutrier-Morello C, *et al*: Identification of variants of the ryanodine receptor type 1 in patients with exertional heat stroke and positive response to the malignant hyperthermia *in vitro* contracture test. *Br J Anaesth* 116: 566-568, 2016.
- Yang M, Zhang Y, Zhao Y and Kang H: Research progress in the multiple organ dysfunction syndrome caused by heat stroke. *Zhonghua Wei Zhong Bing Ji Jiu Yi Xue* 29: 188-192, 2017 (In Chinese).
- Chen CM, Hou CC, Cheng KC, Tian RL, Chang CP and Lin MT: Activated protein C therapy in a rat heat stroke model. *Crit Care Med* 34: 1960-1966, 2006.
- Ren MQ, Kazman JB, Abraham PA, Atias-Varon D, Heled Y and Deuster PA: Gene expression profiling of humans under exertional heat stress: Comparisons between persons with and without exertional heat stroke. *J Therm* 85: 102423, 2019.
- Lumlertgul D, Chuaychoo B, Thitiarchakul S, Srimahachota S, Sangchun K and Keoplung M: Heat stroke-induced multiple organ failure. *Ren Fail* 14: 77-80, 1992.
- Deutsch M, Koskinas J, Emmanuel T, Kountouras D and Hadziyannis S: Heat stroke and multi-organ failure with liver involvement in an asylum-seeking refugee. *J Emerg Med* 31: 255-257, 2006.
- McGeehin MA and Mirabelli M: The potential impacts of climate variability and change on temperature-related morbidity and mortality in the United States. *Environ Health Perspect* 109 (Suppl 2): S185-S189, 2001.
- Bouchama A and Knochel JP: Heat stroke. *N Engl J Med* 346: 1978-1988, 2002.
- Woodrow G, Brownjohn AM and Turney JH: The clinical and biochemical features of acute renal failure due to rhabdomyolysis. *Ren Fail* 17: 467-474, 1995.
- Chen GM, Chen YH, Zhang W, Yu Y, Chen JH and Chen J: Therapy of severe heatshock in combination with multiple organ dysfunction with continuous renal replacement therapy: A clinical study. *Medicine (Baltimore)* 94: e1212, 2015.
- Inoue N, Sato A, Ikawa Y, Shimizu M, Okajima M, Taniguchi T and Yachie A: Successful treatment of exertional heat stroke using continuous plasma diafiltration. *J Clin Apher* 31: 490-492, 2016.
- Hamaya H, Hifumi T, Kawakita K, Okazaki T, Kiridume K, Shinohara N, Abe Y, Takano K, Hagiike M and Kuroda Y: Successful management of heat stroke associated with multiple-organ dysfunction by active intravascular cooling. *Am J Emerg Med* 33: 124.e5-e7, 2015.
- Ye J, Mo W, Chen Y and Yang A: An analysis of laboratory results of parameters of organ function in patients with heat stroke. *Zhonghua Wei Zhong Bing Ji Jiu Yi Xue* 27: 658-661, 2015 (In Chinese).
- Zhao JJ, Zhou JJ, Hu J, Zhou FH, Kang HJ, Liu H, Pan L and Song Q: Analysis of risk factors affecting prognosis of exertional heat stroke. *Zhonghua Wei Zhong Bing Ji Jiu Yi Xue* 25: 515-518, 2013.
- Segev G, Bruchim Y, Berl N, Cohen A and Aroch I: Effects of fenoldopam on kidney function parameters and its therapeutic efficacy in the management of acute kidney injury in dogs with heatstroke. *J Vet Intern Med* 32: 1109-1115, 2018.
- Peng N, Geng Y, Zhang S, Tang Y, Wen Q, Tong H, Liu Y, Liu Z and Su L: Correlation of kidney injury and inflammatory response in rats with classic severe heatstroke. *Zhonghua Wei Zhong Bing Ji Jiu Yi Xue* 27: 327-331, 2015 (In Chinese).

22. Protasi F, Paolini C and Dainese M: Calsequestrin-1: A new candidate gene for malignant hyperthermia and exertional/environmental heat stroke. *J Physiol* 587: 3095-3100, 2009.
23. Leon LR and Helwig BG: Heat stroke: Role of the systemic inflammatory response. *J Appl Physiol* (1985) 109: 1980-1988, 2010.
24. Roberts GT, Ghebeh H, Chishti MA, Al-Mohanna F, El-Sayed R, Al-Mohanna F and Bouchama A: Microvascular injury, thrombosis, inflammation, and apoptosis in the pathogenesis of heatstroke: A study in baboon model. *Arterioscler Thromb Vasc Biol* 28: 1130-1136, 2008.
25. Rosendal L, Langberg H, Skov-Jensen A and Kjaer M: Incidence of injury and physical performance adaptations during military training. *Clin J Sport Med* 13: 157-163, 2003.
26. Yang PC, He SH and Zheng PY: Investigation into the signal transduction pathway via which heat stress impairs intestinal epithelial barrier function. *J Gastroenterol Hepatol* 22: 1823-1831, 2007.
27. Mittal R and Coopersmith CM: Redefining the gut as the motor of critical illness. *Trends Mol Med* 20: 214-223, 2014.
28. Clayton TA, Lindon JC, Cloarec O, Antti H, Charuel C, Hanton G, Provost JP, Le Net JL, Baker D, Walley RJ, *et al*: Pharmaco-metabonomic phenotyping and personalized drug treatment. *Nature* 440: 1073-1077, 2006.
29. Kork F, Holthues J, Hellweg R, Jankowski V, Tepel M, Ohring R, Heuser I, Bierbrauer J, Peters O, Schlattmann P, *et al*: A possible new diagnostic biomarker in early diagnosis of Alzheimer's disease. *Curr Alzheimer Res* 6: 519-524, 2009.
30. Laitano O, Garcia CK, Mattingly AJ, Robinson GP, Murray KO, King MA, Ingram B, Ramamoorthy S, Leon LR and Clanton TL: Delayed metabolic dysfunction in myocardium following exertional heat stroke in mice. *J Physiol* 598: 967-985, 2020.
31. Li Y, Zhu X, Zhang M, Tong H and Su L: Heatstroke-induced hepatocyte exosomes promote liver injury by activating the NOD-like receptor signaling pathway in mice. *PeerJ* 7: e8216, 2019.
32. Tai PA, Chang CK, Niu KC, Lin MT, Chiu WT and Lin JW: Reduction of ischemic and oxidative damage to the hypothalamus by hyperbaric oxygen in heatstroke mice. *J Biomed Biotechnol* 2010: 609526, 2010.
33. Umemura Y, Ogura H, Matsuura H, Ebihara T, Shimizu K and Shimazu T: Bone marrow-derived mononuclear cell therapy can attenuate systemic inflammation in rat heatstroke. *Scand J Trauma Resusc Emerg Med* 26: 97, 2018.
34. Yeh CH, Chen ZC, Hsu CC, Lin MT and Chen CC: Protection in rats with heatstroke: Hyperbaric oxygen vs activated protein C therapy. *Eur J Pharmacol* 635: 103-108, 2010.
35. Yayi H, Yeda X, Huaxin W, Yang W, Qian S and Zhongyuan X: Toll-like receptor 7 involves the injury in acute kidney ischemia/reperfusion of STZ-induced diabetic rats. *Acta Cir Bras* 31: 448-455, 2016.
36. Satirapoj B, Kongthaworn S, Choovichian P and Supasyndh O: Electrolyte disturbances and risk factors of acute kidney injury patients receiving dialysis in exertional heat stroke. *BMC Nephrol* 17: 55, 2016.
37. López-Ibáñez J, Pazos F and Chagoyen M: MBROLE 2.0-functional enrichment of chemical compounds. *Nucleic Acids Res* 44 (W1): W201-W204, 2016.
38. Kanehisa M, Sato Y, Furumichi M, Morishima K and Tanabe M: New approach for understanding genome variations in KEGG. *Nucleic Acids Res* 47 (D1): D590-D595, 2019.
39. Alele F, Malau-Aduli B, Malau-Aduli A and Crowe M: Systematic review of gender differences in the epidemiology and risk factors of exertional heat illness and heat tolerance in the armed forces. *BMJ Open* 10: e031825, 2020.
40. Li L, Tan H, Zou Z, Gong J, Zhou J, Peng N, Su L, Maegele M, Cai D and Gu Z: Preventing necroptosis by scavenging ROS production alleviates heat stress-induced intestinal injury. *Int J Hyperthermia* 37: 517-530, 2020.
41. Thongprayoon C, Qureshi F, Petnak T, Cheungpasitporn W, Chewcharat A, Cato LD, Boonpheng B, Bathini T, Hansrivijit P, Vallabhajosyula S and Kaewput W: Impact of acute kidney injury on outcomes of hospitalizations for heat stroke in the United States. *Diseases* 8: 28, 2020.
42. Weigand K, Riediger C, Stremmel W, Flechtenmacher C and Encke J: Are heat stroke and physical exhaustion underestimated causes of acute hepatic failure? *World J Gastroenterol* 13: 306-309, 2007.
43. Hu J, Kang HJ, Liu C, Hu P, Yang MM and Zhou FH: Response of regulatory T cells to classic heat stroke in mice. *Exp Ther Med* 16: 4609-4615, 2018.
44. Shapiro Y, Alkan M, Epstein Y, Newman F and Magazanik A: Increase in rat intestinal permeability to endotoxin during hyperthermia. *Eur J Appl Physiol Occup Physiol* 55: 410-412, 1986.
45. Gathiram P, Wells MT, Raidoo D, Brock-Utne JG and Gaffin SL: Portal and systemic plasma lipopolysaccharide concentrations in heat-stressed primates. *Circ Shock* 25: 223-230, 1988.
46. Gathiram P, Wells MT, Brock-Utne JG and Gaffin SL: Antilipopolysaccharide improves survival in primates subjected to heat stroke. *Circ Shock* 23: 157-164, 1987.
47. Huisse MG, Pease S, Hurtado-Nedelec M, Arnaud B, Malaquin C, Wolff M, Gougerot-Pocidallo MA, Kermarrec N, Bezeaud A, Guillin MC, *et al*: Leukocyte activation: The link between inflammation and coagulation during heatstroke. A study of patients during the 2003 heat wave in Paris. *Crit Care Med* 36: 2288-2295, 2008.
48. Tong HS, Tang YQ, Chen Y, Qiu JM, Wen Q and Su L: Early elevated HMGB1 level predicting the outcome in exertional heatstroke. *J Trauma* 71: 808-814, 2011.
49. Pozner RG, Ure AE, Jaquenod de Giusti C, D'Atri LP, Italiano JE, Torres O, Romanowski V, Schattner M and Gómez RM: Junin virus infection of human hematopoietic progenitors impairs in vitro proplatelet formation and platelet release via a bystander effect involving type I IFN signaling. *PLoS Pathog* 6: e1000847, 2010.
50. Chen HS, Tong HS, Zhao Y, Hong CY, Bin JP and Su L: Differential expression pattern of exosome long non-coding RNAs (lncRNAs) and MicroRNAs (miRNAs) in vascular endothelial cells under heat stroke. *Med Sci Monit* 24: 7965-7974, 2018.
51. Thulesius O: Thermal reactions of blood vessels in vascular stroke and heatstroke. *Med Princ Pract* 15: 316-321, 2006.
52. Fan H, Zhao Y, Zhu JH, Song FC, Ye JH, Wang ZY and Le JW: Thrombocytopenia as a predictor of severe acute kidney injury in patients with heat stroke. *Ren Fail* 37: 877-881, 2015.
53. Michels S, Buchholz HG, Rosar F, Heinrich I, Hoffmann MA, Schweiger S, Tüscher O and Schreckenberger M: 18F-FDG PET/CT: An unexpected case of Huntington's disease. *BMC Neurol* 19: 78, 2019.
54. Wan Y, Sun SS, Fu HY, Xu YK, Liu Q, Yin JT and Wan B: Adjuvant rhubarb alleviates organs dysfunction and inhibits inflammation in heat stroke. *Exp Ther Med* 16: 1493-1498, 2018.
55. Yang TH, Shih MF, Wen YS, Ho WY, Leu KL, Wang MY and Liu CC: Attenuation of circulatory shock and cerebral ischemia injury in heat stroke by combination treatment with dexamethasone and hydroxyethyl starch. *Exp Transl Stroke Med* 2: 19, 2010.
56. Kurts C, Panzer U, Anders HJ and Rees AJ: The immune system and kidney disease: Basic concepts and clinical implications. *Nat Rev Immunol* 13: 738-753, 2013.
57. Chen Q, Guan X, Zuo X, Wang J and Yin W: The role of high mobility group box 1 (HMGB1) in the pathogenesis of kidney diseases. *Acta Pharm Sin B* 6: 183-188, 2016.
58. Liu GQ, Zuo XH, Jiang LN, Zhang YP, Zhang LM, Zhao ZG and Niu CY: Inhibitory effect of post-hemorrhagic shock mesenteric lymph drainage on the HMGB1 and RAGE in mouse kidney. *Ren Fail* 38: 131-136, 2016.
59. Miriyala S, Thippakorn C, Chaiswing L, Xu Y, Noel T, Tovmasyan A, Batinic-Haberle I, Vander Kooi CW, Chi W, Latif AA, *et al*: Novel role of 4-hydroxy-2-nonenal in AIFm2-mediated mitochondrial stress signaling. *Free Radic Biol Med* 91: 68-80, 2016.
60. Qin S, Wang H, Yuan R, Li H, Ochani M, Ochani K, Rosas-Ballina M, Czura CJ, Huston JM, Miller E, *et al*: Role of HMGB1 in apoptosis-mediated sepsis lethality. *J Exp Med* 203: 1637-1642, 2006.
61. Adato B, Dubnov-Raz G, Gips H, Heled Y and Epstein Y: Fatal heat stroke in children found in parked cars: Autopsy findings. *Eur J Pediatr* 175: 1249-1252, 2016.
62. Xu L, Zhao K, Shen X, Fan XX, Ding K, Liu RM and Wang F: Blockade of extracellular high-mobility group box 1 attenuates systemic inflammation and coagulation abnormalities in rats with acute traumatic coagulopathy. *Med Sci Monit* 22: 2561-2570, 2016.
63. Xiao G, Yuan F, Geng Y, Qiu X, Liu Z, Lu J, Tang L, Zhang Y and Su L: Eicosapentaenoic acid enhances heatstroke-impaired intestinal epithelial barrier function in rats. *Shock* 44: 348-356, 2015.
64. Wei W, Chen M, Zhu Y, Wang J, Zhu P, Li Y and Li J: Down-regulation of vascular HMGB1 and RAGE expression by n-3 polyunsaturated fatty acids is accompanied by amelioration of chronic vasculopathy of small bowel allografts. *J Nutr Biochem* 23: 1333-1340, 2012.
65. Ying S, Xiao X, Chen T and Lou J: PPAR ligands function as suppressors that target biological actions of HMGB1. *PPAR Res* 2016: 2612743, 2016.

